International Journal of Mass Spectrometry 280 (2009) 78–84

Contents lists available at ScienceDirect

International Journal of Mass Spectrometry

journal homepage: www.elsevier.com/locate/ijms

Fragmentation of size-selected Xe clusters: Why does the monomer ion channel dominate the Xe_n and Kr_n ionization?

Viktoriya Poterya [a], Michal Fárník [a,*], Udo Buck [b], David Bonhommeau [c], Nadine Halberstadt [d]

[a] J. Heyrovský Institute of Physical Chemistry, v.v.i., Academy of Sciences of the Czech Republic, Dolejškova 3, 18223 Prague 8, Czech Republic
[b] Max-Planck Institut für Dynamik und Selbstorganisation, Bunsenstr. 10, D-37073 Göttingen, Germany
[c] University of Minnesota, 207 Pleasant Street S.E., 230 Smith Hall, Minneapolis, MN 55455-0431, USA
[d] Laboratoire des Collisions, Agrégats, Réactivite, IRSAMC, UMR 5589, CNRS et Université de Toulouse, F-31062 Toulouse Cedex 09, France

ARTICLE INFO

Article history:
Received 25 May 2008
Received in revised form 10 July 2008
Accepted 18 July 2008
Available online 31 July 2008

PACS:
36.40.Qv
36.40.Wa
36.30.+h
36.40. −c

Keywords:
Cluster
Fragmentation
Ionization
Molecular beam scattering

ABSTRACT

The fragmentation of the small Xe_n $n = 2 - 5$ clusters following 70 eV electron impact ionization has been investigated in a size selective experiment and simulated using non-adiabatic dynamics. The experimental results show that the clusters strongly fragment to yield monomer Xe^+ (more than 90%) and dimer Xe_2^+ fragments (the remaining few percent). Trimer Xe_3^+ fragments first occur from the neutral pentamers Xe_5 in a very low yield of approximately 0.3%. The present results are compared with the previous ones for Kr and Ar clusters. It is shown that the Xe and Kr clusters exhibit a qualitatively similar behavior with a strong propensity for monomer fragments, while in the Ar case dimers prevail. The theoretical calculations also reveal a strong fragmentation to the dimer and monomer fragments. However, the dimer Rg_2^+ is predicted to be the major product for all rare gases (Rg ≡ Ar, Kr, Xe). Possible reasons for the discrepancy between theory and experiment are discussed.

1. Introduction

One of the fundamental issues in mass spectrometry is the fragmentation of a molecule upon electron impact ionization. Many questions remain open, such as how the energy deposited by the ionizing electron into the system is partitioned over the various degrees of freedom of the molecule, how fast does this energy relax, what are the relaxation and/or dissociation pathways, etc. The situation becomes even more complicated when molecular clusters are concerned. They provide many-body systems in which inter as well as intramolecular forces play a role. Therefore the fragmentation of clusters following the interaction with electrons and high-energy photons has been extensively studied in the past [1,2].

In addition, cluster fragmentation upon ionization has practical implications. One of the original and major motivations for cluster investigations has been to shed light on the evolution of cluster properties as a function of their size. In most experiments the cluster size is determined by mass spectrometric methods after ionization. However, the ionization process can lead to the fragmentation and the detected size then does not correspond to the initial neutral cluster size. Therefore it is essential to know the relationship between the measured mass spectrum of the ionized clusters and the neutral precursor cluster size distribution, which is not straightforward in most cases.

Rare gas clusters provide an ideal model system to target these questions. Their relative simplicity allows for high level theoretical treatments, which can bring a detailed understanding of ionization processes at the molecular level when compared to sophisticated size-selective experiments. At the same time rare gas clusters provide benchmark systems for the development of theoretical treatments for many-body systems, which can then be generalized to the more complex molecular species.

Therefore several theoretical and experimental studies have focused in the past on the fragmentation of the rare gas clusters upon ionization. Argon clusters have been by far the most studied systems.[1] In 1984 Buck and Meyer [3] published their

* Correspondingauthor. Tel.: +420 266 053206; fax: +420 286 582307.
E-mail address: michal.farnik@jh-inst.cas.cz (M. Fárník).

[1] Apart from helium droplets, which exhibit very different and original properties and are not discussed here.

1387-3806/$ – see front matter © 2008 Elsevier B.V. All rights reserved.
doi:10.1016/j.ijms.2008.07.024

rather ingenious method for neutral clusters size selection in a crossed-beam experiment, which will be discussed in more detail in the experimental section below. In their experiment [4] they first determined the fragmentation probabilities f_{nk} of neutral Ar_n clusters to ionized Ar_k^+ fragments for $n = 2-6$ and $k = 1-3$ following a 70 eV electron impact ionization. Fragmentation studies of various molecular clusters [5,6] soon followed the argon cluster study. More recently, the size selection scattering method has been modified by using a velocity selector [7] and the fragmentation measurements of Ar_n clusters have been extended up to $n = 9$.

Despite the detailed and partly surprising experimental results, theoretical calculations on the fragmentation of ionized rare gas clusters remained quite rare. The first ones relied on the hypothesis that fragmentation was due to the relaxation of the dimer ion initially formed far from equilibrium by ionization [8,9]. Subsequent classical dynamics showed an appreciable boiling off of argon atoms. These results were confirmed by Stampfli [10] using classical dynamics on the ground electronic state of the ionic cluster. The first non-adiabatic calculation included the lowest three adiabatic states using the classical path surface hopping trajectory method [11]. In Ref. [11] mostly dimer fragments were found, whereas in the experiment dimers are more abundant but monomer ions are also found. The first study taking into account all the potential-energy surfaces involved in the dynamics was carried out for Ar_3 and Ar_4 using a diatomics-in-molecules (DIM) model for the electronic hamiltonian and mean-field ("hemiquantal") dynamics [12], and gave a good agreement with the experiment.

New, more accurate theoretical methods have been developed and were able to model the fragmentation of argon clusters [13] up to $n = 13$. The agreement between theory and experiment is good. In particular, both theory and experiment find that the trimer Ar_3^+ channel opens first for the neutral pentamers $n = 5$. In addition, the main ionic fragments are monomers and dimers with the Ar_2^+ channel being the dominant one.

This was expected to be a general pattern for the behavior of all rare gas clusters, since the ionized dimer has by far the largest binding energy [14–16,9,8]. Indeed, simulations on neon, argon, and krypton clusters [13,17–19] all find ionized dimers to be the most abundant fragments up to $n = 11$. Also another recent theoretical study [20] on the dissociative ionization of Rg_3 (Rg = Ar, Kr, Xe) with a different theoretical method did not reveal important differences in the fragmentation patterns between the various rare gas clusters.

However, a recent experimental study of Kr_n cluster fragmentation [21] disproved this assumption. Ionized krypton clusters fragment almost exclusively to monomers: the Kr^+ channel represents over 90% of the fragments for $n = 1-7$, with very little size dependence. The trimers Kr_3^+ appear first from Kr_5, in accord with the argon case. The theoretical investigations [18] also predict strong fragmentation: if the Kr^+ and Kr_2^+ fragment populations are added, the theoretical results agree quite well with the experimental ones. However, in contrast to the experiment Kr_2^+ is the dominant fragment for $n = 3-11$ with a maximum probability of 84% for $n = 6$. For $n = 3-6$, Kr^+ is the second most populated channel, while for $n \geq 7$ Kr_3^+ exceeds the population of Kr^+. Including spin-orbit couplings in the calculations leads to a smaller relative percentage of Kr_2^+ over Kr^+, with Kr_2^+ still remaining the major product.

Possible sources for these discrepancies have been sought for both in the experiment and in the calculations but no conclusive explanation has been found [19]. Hence a huge discrepancy remains between a sophisticated experiment and high-level theoretical calculations: while theory predicts the Kr_2^+ ionic core to be the major fragment, the experimentally measured fragmentation is by far dominated by Kr^+. What is the reason for this discrepancy? Why is the Kr case so different from Ar?

In this contribution we bring further evidence that monomers are the dominant ionic fragment species for heavier rare gas clusters by measuring the fragmentation of xenon clusters. We find that, like krypton clusters, they fragment almost exclusively to monomer ions. Besides, we show experimentally that the difference between Ar and Xe cluster fragmentation is not just an experimental artifact. We also run non-adiabatic dynamics simulations and predict that Xe_2^+ should be the most abundant fragment from the theoretical point of view in the size range studied. Trimer fragments start appearing for the same size as in the experiment ($n = 5$) although with a somewhat larger percentage. Hence it is confirmed that there is a disagreement between experiment and theory on the proportion of ionic monomer fragments. The hypotheses on which the theoretical treatment is based are examined and several possible sources for the disagreement are proposed.

2. Experiment

The original scattering method introduced in 1984 by Buck and Meyer [3] has been employed for the fragmentation probability measurements in the present study. The method has been described quite a few times since then [4–6], most recently in connection with the krypton cluster fragmentation study [21], and therefore only a brief overview is given below.

The experimental apparatus has been described in more details elsewhere [7,22]. The apparatus was first employed in the fragmentation studies of Ar_n clusters, using a somewhat different method implementing a velocity selector to fully size-select the cluster beam prior to the ionization [7]. The apparatus has been later on slightly modified for photolysis experiments of molecules in cluster environments [22], and it has recently been moved from Göttingen to Prague, where it is employed for similar photodissociation studies. Since the apparatus offers the option of a secondary crossed beam with time of flight analysis, it can be used for size selection as in the original Buck–Meyer method without the velocity selector [4]. This option has been exploited in our recent study of pyrrole clusters [23]. It was also used in the early stage of the fragmentation studies on krypton clusters. Because of the surprising nature of the results, the experiments were continued in the original Buck–Meyer [4] apparatus. The fragmentation probabilities turned out to be almost identical in both machines and underline the reliability of the present setup.

Fig. 1 shows schematically the present experimental setup. Xenon clusters are produced in a xenon gas expansion through a conical nozzle of 60 μm diameter, 2 mm length, and 30° opening angle at a stagnation pressure of 2 bar and a temperature of 273 K. The helium beam is produced by expanding 30 bar room-temperature helium through a 30 μm diameter pinhole. Both beams pass through skimmers into a differentially pumped scattering chamber, where they intersect at 90°. The whole assembly is connected with a flexible bellow to the next vacuum chamber, and can be rotated to a given angle in the horizontal plane, allowing the xenon clusters scattered at that angle to proceed along their path to detection. The scattered part of the primary beam enters the next

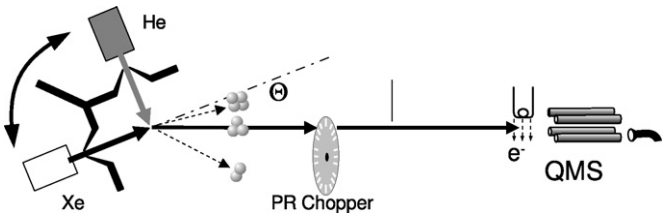

Fig. 1. Schematic view of the experimental apparatus.

chamber, passes through a pseudo-random chopper and proceeds further into the following two ultra-high vacuum chambers. In the latter one the beam is electron impact ionized and analyzed by means of a quadruple mass-spectrometer. Ionization of the beam is performed with 70 eV electrons at ≈10 mA.

The scattering analysis provides a unique correlation between the detected cluster ion and its neutral precursors, independent of the cluster size distribution in the primary beam and the fragmentation process in the ion source [4]. The method relies on the specific kinematic behavior of clusters with different sizes scattered from a target beam. From the so-called Newton diagram discussed in more details elsewhere (e.g. in Ref. [4]), it follows that under typical experimental conditions with a moderate energy transfer during collision, each Xe_n cluster could be scattered in the laboratory (LAB) system only within a certain angular range. The tangent to the corresponding circle determines the maximum LAB scattering angle Θ_n to which size n clusters can be deflected. Setting the detector to a larger scattering angle $\Theta > \Theta_n$ implies that only clusters with size smaller than n can reach the detector.

In our experiment two types of measurements are usually performed. First, the angular distribution for the sequence of ionic fragments $k = 1, 2, \ldots$ is measured. The intensity of the detected signal S_k at a given angle Θ is the sum of the contributions from all the neutral precursors which can be scattered at that angle.

$$S_k(\Theta) = \sum_{n=k}^{n_{\max}(\Theta)} N_{nk}(\Theta). \tag{1}$$

The second type of measurements is time-of-flight (TOF) measurements in which a pseudorandom chopper is used in conjunction with the quadrupole mass spectrometer to measure the time dependent signal of a particular ion mass, i.e. the velocity distribution. From the Newton diagram it follows that the neutral clusters with sizes allowed at a given scattering angle ($n \le n_{\max}(\Theta)$) arrive with different velocities depending on their size. By measuring the TOF distributions the relative integrated intensities X_{nk} can be determined

$$X_{nk}(\Theta) = \frac{N_{nk}(\Theta)}{\sum_{n=k}^{n_{\max}(\Theta)} N_{nk}(\Theta)}, \tag{2}$$

where the sum in the denominator represents an integral of the measured TOF spectrum over the final LAB velocity. Using Eqs. (1) and (2) the fragmentation probabilities f_{nk} for the neutral cluster of size n to fragment to an ion of size k can be calculated as follows

$$f_{nk} = \frac{S_k X_{nk}}{\sum_{k=1}^{n} S_k X_{nk}}. \tag{3}$$

where the normalization condition is given by $\sum_{k=1}^{n} f_{nk} = 1$. Here f_{nk} is expressed in terms of two measurable quantities, S_k obtained from the angular distributions and X_{nk} from the analysis of the normalized TOF spectra. The probability f_{nk} can be evaluated for different scattering angles and the average values are considered.

3. Experimental results

Fig. 2 represents the angular distribution (differential cross section) $S_k(\Theta)$ measured for the different Xe_k^+ fragments, $k = 1, 2, 3$. The corresponding threshold angles Θ_n for the scattering of the neutral Xe_n clusters, $n = 1, \ldots, 6$ are indicated by vertical dotted lines. Considering the finite angular resolution of $\Delta\Theta \approx 1^\circ$ (FWHM), as determined by the measurement of the angular distribution of

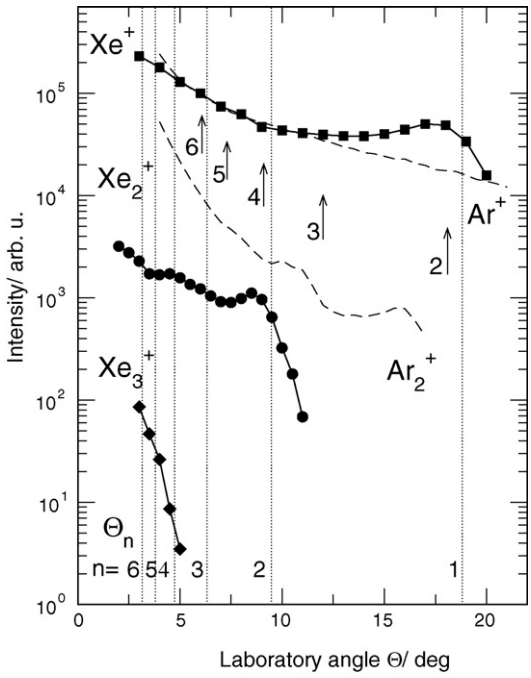

Fig. 2. Measured angular distributions for Xe clusters in collisions with He atoms for fragment ion masses of monomer Xe^+(squares), dimers Xe_2^+ (circles) and trimers Xe_3^+ (diamonds). The distributions for Ar^+ and Ar_2^+ (dashed lines) are included for comparison. The dotted vertical lines indicate positions of the threshold angle for neutral Xe-cluster of the size n. The arrows show the threshold angles for Ar-clusters.

the primary beam, the onsets of the Xe^+ and Xe_2^+ signals are in good agreement with the calculated threshold angles $\Theta_1 = 18.8^\circ$ and $\Theta_2 = 9.7^\circ$, respectively. The maxima close to the threshold angles correspond to singularities in the Jacobian describing the CM → LAB transition [6].

It has already been mentioned in Section 1 that the fragmentation of krypton and xenon clusters differs qualitatively from the fragmentation of argon clusters. Since this conclusion has not been supported by the theoretical calculations so far, it is worth showing that this is not an experimental artifact. Therefore together with the xenon cluster scattering we have also measured the argon cluster angular distribution scattered from He, represented by dashed lines in Fig. 2 for the Ar^+ and Ar_2^+ fragments. The threshold angles for the Ar clusters are indicated by short arrows. Especially the relative ratio of the Ar^+ to the Ar_2^+ distribution is relevant in the present context.

The ratios $S_1(\Theta)/S_2(\Theta)$ of the Rg^+ to Rg_2^+ signal for Rg = Ar, Kr and Xe are compared in Fig. 3. The x-axis corresponds to the scattering angle normalized to the trimer threshold angle Θ/Θ_3 for each rare gas, i.e. $\Theta_3 = 12.1^\circ$ for Ar, 8.2° for Kr and 6.3° for Xe. It can be seen that the ratio for Kr and Xe behaves very similarly: it is around 100 and almost constant over the angular range. This is quite different from the Ar case, where this ratio is 10 times smaller for small scattering angles and increases gradually so that it is approximately 2.5 times smaller close to the trimer threshold angle. This is part of the reason for the much larger values of the f_{n2} fragmentation probabilities for the Ar case since, as can be seen from Eq. (3), $f_{n1}/f_{n2} = [S_1(\Theta)/S_2(\Theta)] \times [X_{n1}(\Theta)/X_{n2}(\Theta)]$. Indeed, this is only part of the reason. There are also differences in the X_{nk} values between Ar and Xe (Kr) clusters scattering (see the velocity distributions below from which they are deduced and those in Refs. [21,4]). Hence there is a significant qualitative difference in the fragmentation behavior of Ar and Xe (Kr) clusters. The similarity in the measured differential cross section for Xe and Kr and their difference to the Ar ones show that the difference in

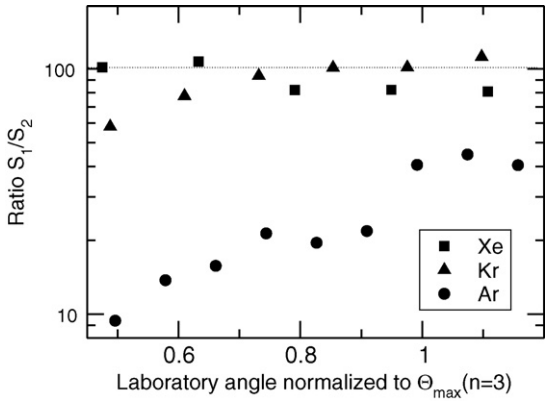

Fig. 3. Ratio of the monomer to dimer ion signal for the three different rare gases: Ar, Kr, Xe. The *x*-axis corresponds to the scattering angle normalized to the trimer threshold angle Θ/Θ_3 for each particular rare gas, i.e. $\Theta_3 = 12.1^\circ$, 8.2°, 6.3° for Ar, Kr and Xe respectively.

fragmentation probabilities between argon and the heavier rare gas clusters cannot be just an experimental artifact.

Another feature to be noted about the angular distribution in Fig. 2 is that the Xe_3^+ signal approximately appears at the threshold angle for the pentamers Xe_5. This implies that the trimer fragment first occurs from the pentamer, which is again in agreement with the Kr case. Note that this was also true for the argon case. It ought to be mentioned that although the fragmentation probability $f_{53} = 0.3 \pm 0.2\%$ evaluated from the TOF spectra below is extremely small, the angular distribution suggests that there are at least some Xe_3^+ fragments originating from the Xe_5 clusters.

Next the TOF spectra were measured at 10 different LAB angles for the two major fragments Xe^+ and Xe_2^+. To calculate the fragmentation probabilities for each cluster size, the measured TOF spectra were analyzed for contributions from the various neutral clusters. An example of this analysis is shown in Fig. 4. The measured data are represented by circles, and the solid lines are the results of the fit by the sum of contributions from relevant neutral cluster sizes using a nonlinear least-squares fit method. We note that the only fitting parameters are the peak intensities. The number and positions of the fitted peaks are determined by the

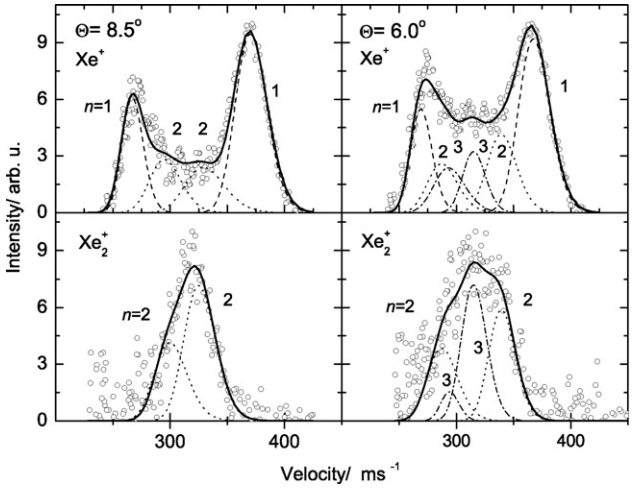

Fig. 4. Velocity distributions at $\Theta = 8.5^\circ$ (left panels) and 6.0° (right) measured at the mass of monomer ion Xe^+ (top) and dimer ion Xe_2^+ (bottom). The circles show the measured data, the solid line shows the fit by the sum of contributions from the relevant neutral cluster sizes Xe_n, $n = 1$ (dashed line), $n = 2$ (dotted line) and $n = 3$ (dashed-dotted line).

Table 1
Fragmentation probabilities f_{nk}: $(Xe)_n \rightarrow (Xe)_k^+$: comparison between experimental and theoretical results

n	$k=1$	$k=2$	$k=3$	
2	0.96(3)	0.04(2)	-	exp.
	0.44	0.56	-	theo.
3	0.94(4)	0.06(3)	-	exp.
	0.29	0.71	0.0	theo.
4	0.97(4)	0.03(2)	-	exp.
	0.22	0.76	0.007	theo.
5	0.97(5)	0.027(15)	0.003(2)	exp.
	0.16	0.74	0.07	theo.

The number in parentheses represents the estimated experimental error.

scattering kinematics and hence are calculated from the Newton diagram. The peak shapes and half widths are derived from the measurement of the primary and secondary beam velocities and angular distributions.

The measured TOF spectra have been converted to velocity distributions. Fig. 4 shows the distributions at $\Theta = 8.5^\circ$ and 6.0°. Since $\Theta = 8.5^\circ$ is beyond the trimer threshold angle, only the monomers and dimers are expected to contribute. Therefore the Xe^+ spectrum (top panel) has been analyzed for contributions from the neutral monomer (dashed lines) and the neutral dimer Xe_2 (dotted lines). The pairs of peaks correspond to the forward and backward scattered clusters in the CM system. Similarly only the neutral dimer Xe_2 (dotted lines) was taken into account in the Xe_2^+ spectrum (bottom panel) analysis. Right panels of Fig. 4 illustrate the increasing number of contributing neutral clusters when going to smaller scattering angles. These spectra have been measured at $\Theta = 6.0^\circ$, which is below the trimer threshold angle but still beyond the tetramer one. Therefore the neutral trimer contribution is also considered in the fits (dashed-dotted lines).

The fragmentation probabilities f_{nk} were calculated from the X_{nk} values obtained in the fitting procedure. They are collected in Table 1. The values were calculated for each measured laboratory angle and then averaged. The results were in close agreement, which is a good consistency check of the data evaluation procedure. The number in parenthesis indicates the experimental error estimated from the different scattering angles. The present results are also in agreement with a sophisticated data evaluation procedure based on a Monte Carlo (MC) simulation, which takes into account the kinematics of cluster scattering, the beam divergences, the velocity distributions of the two beams, and the resolution of the TOF analyzer [4,21].

4. Dynamics calculations

It was already mentioned in Section 1 that the theory and experiment agree well on the fragmentation pattern for argon clusters [13], but that differences appear for the heavier krypton clusters. In order to ascertain what is the level of discrepancy between theory and experiment, we have performed a non-adiabatic study of the fragmentation dynamics of xenon clusters upon ionization. This study is similar to the ones already performed for neon, argon and krypton clusters [13,18,19]. It takes into account all the electronic states correlating asymptotically to $Xe^+(^2P_{3/2})$ or $Xe^+(^2P_{1/2}) + (n-1)$ Xe and their couplings, including spin-orbit coupling. The dynamics is described using a mixed quantum-classical method in which nuclei are treated classically and electrons (here the electronic hole) quantum mechanically. The nuclei evolve on one of the adiabatic potential energy surfaces. The multi-surface aspect of the problem is taken into account by letting the nuclei change surface ("surface hops") at any time with a probability governed by the time evolution of the electronic state probabilities in the quantum wave

packet propagation. The DIM model, with the addition of induced dipole-induced dipole and spin–orbit interactions, has been used by a number of authors before to describe ionized rare gas clusters [24–27,20]. It has been shown to be very accurate for these systems [28]. It is used here to determine "on the fly" potential energy surfaces and their couplings. The input curves are taken from Refs. [29,30].

The following assumptions are made. Electron impact ionization performed with ~70 eV electrons is very fast (less than a femtosecond) compared to any nuclear motion (electrons at that energy travel at ~50 Å fs^{-1}). Therefore it is assumed to be "vertical", i.e. instantaneous and for fixed positions of the nuclei. The excess energy is assumed to be shared between the ionizing and the departing electrons so that the momenta (velocities) of the nuclei are also unchanged. Since the energy width associated with subfemtosecond excitation is of several eV, 70 eV electron impact ionization is assimilated to coherent white light ionization and all electronic states are populated. In addition there are no transition dipole moment rules so every electronic state of the ion is initially equiprobable. Initial positions and momenta of the nuclei are determined by running a classical trajectory for the neutral cluster at its zero-point energy and (after an equilibration period) assuming a vertical ionization at a given time interval.

The results of this simulation are confronted to the experimental ones in Table 1. Xenon clusters behave like the other rare gas clusters, with dimer ions being the main fragments. Their proportion increases with initial cluster size up to a maximum and then decreases again to the profit of trimer ion fragments. This maximum proportion is already obtained for $n = 4$ (76%). It was at $n = 8 - 10$ (99%) for neon [17], $n = 6$ (95%) for argon [13], and $n = 6$ (84%) for krypton [18]. The next more abundant ionic fragments are monomers for the size range studied. Their proportion decreases from 44% for $n = 2$ to 16% for $n = 5$. Trimers start appearing for $n = 4 - 5$.

The simulation clearly does not reproduce the predominance of monomer fragment ions. The highest Xe^+ proportion comes from Xe_2 and it is only 44%. In addition, its proportion decreases with initial cluster size, while the experimental one is about constant within experimental uncertainty.

It ought to be mentioned that the fact that the simulations for all the rare gas clusters (Ne, Ar, Kr and Xe) yield very similar results is not surprising since the parameters are not very different. In particular the dissociation energy for one atom from the n-cluster is largest for the dimer. There is an evolution with mass and spin-orbit but no discontinuity. Thus if we want to reproduce the abrupt change seen in experiment between Ar and Kr–Xe a qualitatively new phenomenon has to be introduced in the simulations.

5. Discussion

As in the previously studied krypton case, the comparison of the measured and calculated fragmentation probabilities for Xe_n clusters reveals a large discrepancy concerning the proportion of monomer fragment ions, starting already from the neutral dimer. Possible sources for these discrepancies have been sought for both in the experiment and in the calculations and also partly discussed in a recent joint theoretical–experimental review [19]. In this review a correction of the measured fragmentation probabilities was proposed, which was based on the fact that the fragmentation was very fast (of the order of a picosecond) compared to the time of flight in the ionization region. Hence it was conjectured that most of the neutral monomer fragments could still be ionized. This is, however, a very improbable event given the very low ionization probability of the order of 10^{-3}.

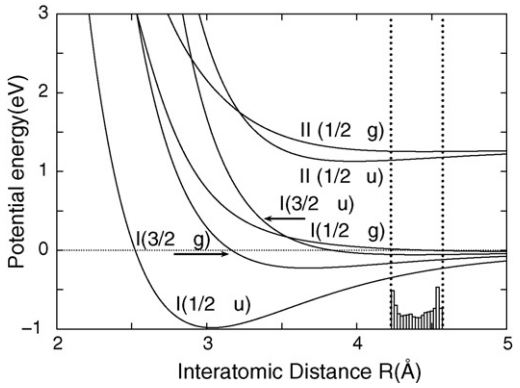

Fig. 5. Xe_2^+ potential energy curves used in this calculation. The histogram represents r (Xe–Xe distance) initial conditions for Xe_2 ionization dynamics.

Thus we are still left with the large discrepancy between theory and experiment concerning the amount of monomers in the fragmentation dynamics, which is mainly observed for the Kr and Xe clusters[2] and which occurs already for the fragmentation of the neutral dimers.

Let us focus on the dimer parent ion. It can only fragment if it is created with an energy above the $Xe^+(^2P_{3/2}) + Xe$ dissociation limit. Xe_2^+ has six (doubly degenerate) electronic states, which are presented in Fig. 5. Four states correlate with $Xe^+(^2P_{1/2}) + Xe$ and two with the spin-excited state $Xe^+(^2P_{3/2}) + Xe$. Fig. 5 also shows the initial distribution of distances obtained by vertical ionization from the neutral dimer. In this distance range, 4.2–4.6 Å, both states correlating to the spin-orbit excited state [II(1/2u) and II(1/2g)] are above the dissociation limit, and so is part of the I(1/2g) state (correlating to the ground spin-orbit state). Hence a maximum of 50% dissociation can be obtained. The kinetic energy of the nuclei in the neutral dimer, which is carried as initial condition to the ion since momenta are assumed to be unchanged by ionization, is very small and does not alter this conclusion.

One possibility for the disagreement between theory and experiment would be a preferential population of the states correlating to the spin-orbit excited dissociation limit. Ionization cross sections do have a dependence on generalized oscillator strengths [31] but it remains to be justified why these particular states would be populated with higher probability. Another possibility would be the population of higher electronic states that are not included in the simulation. However, the ionization cross section of Xe in the 5s orbital is about a factor of 10 smaller than that in the 5p orbital [32], and the same ratio can be expected for the dimer, so this could not account for the difference. Using quantum initial conditions could slightly increase the proportion of monomer fragments but not to a large extent. Taking into account the non-zero internal temperature of the neutral dimers will also affect initial conditions, however, preliminary test calculations suggest that this effect is not large.

On the experimental side another possibility is a generation of multiply charged clusters, which can then decay to several monomer fragments. A direct double ionization of a single atom within the cluster is very improbable under the current experimental conditions. For large Ar_n and Xe_n clusters with about 100 and more atoms multiple ionization processes have been observed, which were caused by up to three subsequent single ionization

[2] For Ar the experimental fragmentation probability agrees well with the calculated one for the neutral dimer and trimer, and for the larger clusters $n = 4$ to 9 the measured fragmentation probability to the monomer without any correction is only about 20% higher than the calculated one, i.e. the dimer ion Ar_2^+ still remains the major fragment channel.

events of one incoming electron colliding with different atoms within the cluster even at electron energies below 70 eV [33]. On the other hand, such multiple ionization processes are much less probable in the small clusters concerned here, especially in the dimer. Another multiple ionization process, which is however possible even for dimers, is the recently reported inter-atomic Coulombic decay (ICD) [34]. These processes can occur when inner-valence subshell electrons are removed from the ionized atom and the excess energy of the ion is utilized to ionize the neighboring atom. The cluster with two positively charged atoms then decays via the Coulomb interaction, which can lead to the excess of monomer fragments. To assess the possible monomer contribution from the ICD, the efficiency of these processes with respect to the direct outer-valence electron ionization would have to be known. This cross section might be lower because the inner shell electron is involved [32]. Also, excluding these processes by lowering the ionizing electron energy below twice the ionization potential of the atom is not experimentally feasible, since the ion signals at energies below 50 eV become too small for the current experiment. The dependence on the electron energy between 50 and 100 eV has been measured for Ar clusters, but no significant differences in the fragmentation pattern have been observed.

The energy deposited in the cluster by the ionizing electron deserves a somewhat more detailed discussion. It is possible that in the experiment the excess energy in the ionization process is not completely taken away by the scattered and nascent electrons, and that a certain amount of this energy remains in the cluster. Our simulation takes into account the internal energy deposited in the cluster as potential energy because vertical ionization accesses the ionic potential energy surfaces far from equilibrium. From the initial conditions presented in Fig. 5 we estimate that about 0.3 eV of kinetic energy added to the potential energy would be enough to dissociate almost all the dimers. However, the electron–xenon energy transfer is classically very small due to the very unfavorable mass ratio. Another possibility would be that the ejected electrons could interact with the other cluster electrons. This interaction could lead to additional energy transfer to the parent ion. The internal energy distributions of molecular ions have been determined experimentally for polyatomic molecules up to heptane [35,36]. The energy loss spectra of the incident electrons and the energy of the ejected electrons were measured in a coincidence experiment and internal energy distributions were deduced by energy balance. The results were in agreement with findings obtained from differential ionization efficiency curves. They peak between 0 and 1 eV, have a width of 2–3 eV and a tail up to 5 eV. We have recently also deduced a similar energy distribution with maximum at around 1 eV and a tail extended up to about 5 eV for a 70 eV electron impact ionization of pyrrole clusters [23]. A similar coincidence experiment for electron-Xe_2 scattering would be highly desirable in order to compare the internal energy distribution of the parent ion with that deduced from the assumption of vertical ionization. In parallel, the ionization process itself should be modeled theoretically.

Finally, it is noteworthy that one of the experimental findings here is the qualitative difference in the fragmentation of Xe and Kr clusters with respect to the Ar ones. Therefore a possible clue for solving the puzzle of the high fragmentation rate for Xe and Kr clusters should originate from differences between Ar and the heavier rare gas clusters. However, at the present stage we cannot point out the difference which would conclusively explain the qualitatively different fragmentation behavior.

6. Conclusions

The fragmentation of small Xe_n (n = 2–5) clusters following 70 eV electron impact ionization has been measured in a size selective experiment. The clusters strongly fragment and yield monomer fragments Xe^+ in a proportion larger than 90% for all the measured neutral sizes. The remaining fragments are dimers $Xe_2{}^+$. The trimer $Xe_3{}^+$ fragments first occur from the neutral pentamers Xe_5 in a very small percentage (less than 1%).

These findings have been compared with theoretical calculations performed for this work. While the general picture is similar, namely severe fragmentation to the monomer and dimer ions and the first appearance of the trimer ion for the neutral pentamer, the actual numbers of the fragmentation pattern differ appreciably. The dimer ion $Xe_2{}^+$ is always the most populated fragment with 56%, 71%, 76%, and 74% for the neutral dimers to pentamers, respectively and the amount of trimer ions $Xe_3{}^+$ originating from pentamers is 7%.

The present results have been compared with the previous ones for Kr and Ar clusters. The experimental propensity for monomer ion production for Xe is quite in agreement with the observation for Kr, while the dimer ion has been observed as the major product in the case of Ar both in the experiment and in the theoretical simulations. The comparison of the angular distribution of the different clusters shows that the Xe and Kr clusters behave very similarly, while the Ar clusters exhibit a qualitatively different behavior. Thus it has been demonstrated that the high fragmentation for Xe and Kr clusters is not just an experimental artifact.

Possible reasons for the discrepancy with the theory have been discussed and several hypotheses concerning the theoretical simulations are currently under study.

Acknowledgment

This work is dedicated to Professor Zdenek Herman, who as a great scientist, artist and human being is an inspiration and a good friend to all of us, on the occasion of his 75th birthday.

We would like to acknowledge C. Steinbach for his kind help with the data evaluation. Support by the special program “Nanotechnology for society” of the Czech Academy of Sciences grant Nr.: KAN400400651, and by the Grant Agency of the Czech Republic Grant Nr.: 203/06/1290 is gratefully acknowledged. The cooperation between Prague and Toulouse group has been supported by program KONTAKT-BARRANDE MEB02-07-14. M.F. acknowledges the J.E. Purkyně fellowship of the Czech Academy of Sciences. N.H. and D.B. acknowledge the grant of CPU time from the IDRIS and CALMIP computing centers.

References

[1] T.D. Märk, O. Echt, in: H. Haberland (Ed.), Clusters of Atoms and Molecules II, Springer, Berlin, 1994, p. 154.
[2] T.D. Märk, L.G. Christopherou, Linking the Gaseous and Condensed Phases of Matter, Plenum Press, New York, 1994, p. 155.
[3] U. Buck, H. Meyer, Phys. Rev. Lett. 52 (1984) 109.
[4] U. Buck, H. Meyer, J. Chem. Phys. 84 (1986) 4854.
[5] U. Buck, J. Phys. Chem. 92 (1988) 1023.
[6] U. Buck, in: G. Scoles (Ed.), The Chemical Physics of Atomic and Molecular Clusters, North Holland, Amsterdam, 1990, p. 543.
[7] P. Lohbrandt, R. Galonska, H.J. Kim, M.S.C. Lauenstein, U. Buck, in: R. Campargue (Ed.), Atomic and Molecular Beams. The State of the Art 2000, Springer, Berlin, 2001, p. 623.
[8] J.M. Soler, J.J. Sáenz, N. García, O. Echt, Chem. Phys. Lett. 109 (1984) 71.
[9] J.J. Sáenz, J.M. Soler, N. García, Surf. Sci. 156 (1985) 121.
[10] P. Stampfli, Z. Phys. D 40 (1997) 345.
[11] P.J. Kuntz, J.J. Hogreve, J. Chem. Phys. 95 (1991) 156.
[12] A. Bastida, N. Halberstadt, J.A. Beswik, F.X. Gadéa, U. Buck, R. Galonska, C. Lauenstein, Chem. Phys. Lett. 249 (1996) 1.
[13] D. Bonhommeau, N. Halberstadt, A. Viel, J. Chem. Phys. 124 (2006) 184314.
[14] K. Stephan, T.D. Märk, Chem. Phys. Lett. 90 (1982) 51.
[15] H. Haberland, J. Eichler, L.V. Hertel, N. Stolterfoht, in: J. Eichler, I.V. Hertel, N. Stolterfoth (Eds.), Electronic and Atomic Collisions, North Holland, Amsterdam, 1983.
[16] H. Haberland, Surf. Sci. 156 (1985) 305.

[17] D. Bonhommeau, A. Viel, N. Halberstadt, J. Chem. Phys. 123 (2005) 054316.
[18] D. Bonhommeau, T. Bouissou, N. Halberstadt, A. Viel, J. Chem. Phys. 124 (2006) 164308.
[19] D. Bonhommeau, N. Halberstadt, U. Buck, Int. Rev. Phys. Chem. 26 (2007) 353.
[20] I. Janeček, D. Hrivňák, R. Kalus, F.X. Gadea, J. Chem. Phys. 125 (2006) 104315.
[21] C. Steinbach, M. Fárník, U. Buck, C.A. Brindle, K.C. Janda, J. Phys. Chem. A 110 (2006) 9108.
[22] R. Baumfalk, U. Buck, C. Frischkorn, S.R. Gandhi, C. Lauenstein, Ber. Bunsenges. Phys. Chem. 101 (1997) 606.
[23] V. Profant, V. Poterya, M. Fárník, P. Slavíček, U. Buck, J. Phys. Chem. A 111 (2007) 12477.
[24] J. Heßlich, P.J. Kuntz, Z. Phys. D 2 (1986) 251.
[25] M. Amarouche, G. Durand, J.P. Malrieu, J. Chem. Phys. 88 (1988) 1010.
[26] R. Kalus, D. Hrivňák, Chem. Phys. 278 (2002) 21.
[27] D. Hrivňák, R. Kalus, F.X. Gadéa, Europhys. Lett. 71 (2005) 42.
[28] F.Y. Naumkin, P.J. Knowles, J.N. Murell, Chem. Phys. 193 (1995) 27.
[29] P. Rupper, O. Zehnder, F. Merkt, J. Chem. Phys. 121 (2004) 8279.
[30] A.K. Dham, W.J. Meath, A.R. Allnatt, R.A. Aziz, M.J. Slaman, Chem. Phys. 142 (1990) 173.
[31] E. Gargioni, B. Grosswendt, Rev. Mod. Phys. 80 (2008) 451.
[32] P.L. Bartlett, A.T. Stelbovics, Phys. Rev. A 66 (2002) 012707.
[33] T.D. Märk, Int. J. Mass. Spectrom. Ion Proc. 79 (1987) 1.
[34] R. Santra, J. Zobeley, L.S. Cederbaum, N. Moiseyev, Phys. Rev. Lett. 85 (2000) 4490.
[35] W.A. Chupka, M. Kaminsky, J. Chem. Phys. 35 (1961) 1991.
[36] H. Ehrhardt, F. Linder, Z. Naturforsch. 2a (1967) 444.